

Performance Analysis of PMSM for EV Application Considering Thermal Constraints

Pancham Arun Chaudhari

MASTER IN ELECTRICAL ENGINEERING

KCE Society's College of Engineering and management, jalgoan

Abstract - The impact of varying stator slot size on the efficiency and thermal capabilities of an electric vehicle's permanent magnet synchronous machine is analysed and measured in this research. Finite element analysis was used to analyse an electromagnetic machine with four different sized slot areas, and a lumped parameter network model was used to evaluate a machine with four different sized slot areas thermally. The core losses are reduced due to the broader magnetic path when the slot size is reduced while the other dimensions remain constant, however the winding losses rise. Additionally, due to lower saturation, a greater

maximum torque is achieved. The results are compared in the torque-speed operating area of the machine in terms of machine-part and total losses, continuous torque and transient overload capabilities, and energy losses and peak winding temperature during 19 low, middle, and high-speed drive cycles. The biggest slot had the lowest winding losses and, as a result, the most thermally constrained torque capacity. Due to its lower component load (i.e. core) losses, the energy losses with the biggest slot were the highest in 13 of the drive cycles and the lowest in 11 of them with the smallest slot. Because it has the least copper, the smallest slot would also have the lowest material cost.

Keywords - PMSM, Finite Element Analysis, Lumped Parameter Network.

I. INTRODUCTION

The torque and power rating of an electric machine is generally controlled by the winding

temperature, which damages the insulation and reduces the machine's lifetime. Furthermore, high magnet temperatures increase the danger of demagnetization in permanent magnet devices [1-3].

High performance and efficiency, as well as minimal weight, volume, and cost, are common design goals for propulsion electric machines. Machines in electric vehicles (EVs) typically encounter very dynamic load cycles, resulting in correspondingly changing internal losses and, as a result, temperature changes that are considerably time dependent. Machines are often constructed to tolerate a certain amount of

overload before reaching a critical winding temperature as a trade-off. As a result, in addition to electromagnetic and mechanical assessment, it is critical to address temperature elements of propulsion machines throughout the design phase. The desire to do so has grown in recent years, owing in part to the growing interest in transportation electrification.

It is often considered that the most accurate results in machine modelling and simulation are obtained utilising well-representative computer-aided design (CAD) models and numerical solvers. However, especially for conjugate heat transfer analysis with fluid dynamics, the compute effort required to provide adequate data for assessment is significant. Reduced order thermal models, such as lumped parameter networks (LPN), are easily employed to produce effective characterisation throughout the whole working region, as is required during vehicle drive cycle assessments [2,4].

Multi-objective optimization approaches, in which both geometrical and material characteristics are adjusted in order to meet requirement criteria such as high torque, low losses, torque ripple, and material cost [5,6], are a common electromagnetic machine design procedure. Thermal LPN modelling and assessment are preferable incorporated in the optimization loop to attain these aims [7,8], but it may also be applied to the subsequent optimised design, or a few selected design variants for comparison [9-11].

Alternatively, the design study can concentrate on a specific design feature, such as the pole/slot combination [12], the slot form [13], or external parameters, such as the gear ratio [14], all while evaluating temperature with thermal LPN models. Another technique is to execute numerous single design parameter sweeps in a row, as described in [15].

As shown in [11,12,14], suggested optimal designs are frequently electromagnetically and thermally tested across one or two driving cycles. Occasionally, a few additional driving cycles are employed, as in [5.] where five cycles are concatenated and weighted as a combined input to the optimization.

In brief, a number of publications have been published that offer useful modelling and simulation tools, as well as optimization procedures, for electric machines in electric cars that address thermal factors.

The goal of this work is to assess the influence of a different stator slot size on the electromagnetic efficiency and

thermal capabilities of a permanent magnet synchronous machine (PMSM) for a light-duty (passenger car) battery electric vehicle, building on the concept of targeted design studies (BEV). The temperatures are assessed using a thermal lumped parameter model, with temperature adjusted losses as input, and the electromagnetic losses are analysed using finite element analysis (FEA).

As a result of the narrower magnetic path, it is expected that a greater slot area will result in lower winding losses and higher core losses. As a result, losses can be redistributed between the winding and the core by changing the slot size.

The outside and internal machine dimensions (excluding slot size) are unchanged throughout the research, as are the battery and inverter current and voltage ratings, as well as the transmission's mechanical ratings. Because packaging is normally carefully regulated in the automobile business, this is considered a justifiable scope. Furthermore, a change in one component should ideally not need a change in any of the other drive system components, as this would result in considerable cost increases.

II. REFERENCE MACHINE

A permanent magnet synchronous machine (PMSM) is used as the reference machine since this kind is quite widespread in today's battery electric vehicles (BEVs) [15]. They have a high torque and power density as well as a high efficiency.

The lamination cross section is similar to commercially common designs [16], particularly the Toyota Prius 2004 motor, which has 48 slots, 8 poles, and a v-shaped inner permanent magnet (IPM) structure, as illustrated in Fig. 1. In comparison to the Prius 2004, the stator teeth and yoke are thinner, and the v-shaped magnet arrangement is set at a different angle. Figure 1 also shows a simpler frame with a spiral liquid cooling channel (shown in Fig. 12) and a shaft with two ball bearings.

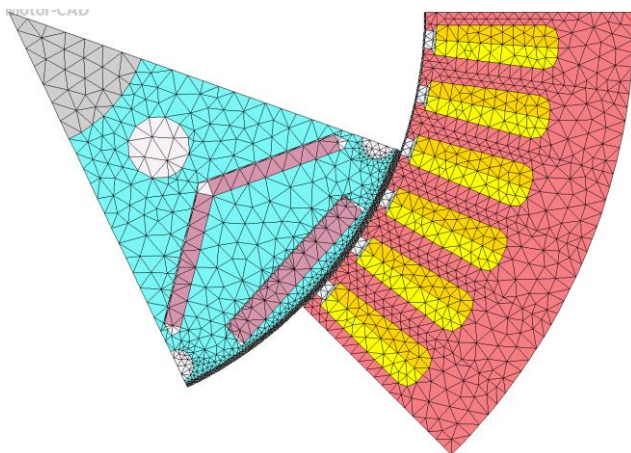


Figure 1: Mesh density of the reference machine

A reference machine (with the Original slot size) is sized to meet the requirements of a large-scale battery electric vehicle (BEV) that has been envisioned. Table 1 shows selected data for this machine. As shown in Fig. 2, four distinct slot areas are explored based on the reference machine: Small, Original, High, and Large. The machine with the Original slot will henceforth be referred to as the reference machine. The Small slot has broader teeth and a thinner yoke, whereas the Large slot has somewhat narrower teeth and a thinner yoke, and the High slot merely has a thinner yoke, as indicated in Table 2. Because the gross copper fill factor is consistent in all situations (within 1%), the winding cross sectional area varies with slot area, as shown in Table 2. This is predicated on the premise that different diameter conductors will be used inside the same coil.

Table 1: Reference Machine Data with Original Slot Size

Parameter	Value, unit
Peak Power	80 kW
Maximum Torque	214 N-m
Base Speed	4000 rpm
Maximum Speed	12000 rpm
Maximum DC Voltage	400 V
Maximum RMS current density	20 A/mm ²
Maximum RMS Phase current	251 A
Core Length	160 mm
Core Stacking Factor	95%
Lamination Thickness	0.3 mm
Number of Slots	48
Number of Poles	8
Stator Outer diameter	198 mm
Stator Inner diameter	132 mm
Stator Yoke thickness	10.4 mm
Tooth width	4.1 mm
Tooth height	21.1 mm
Slot Opening width	2.8 mm
Slot fill factor	45%
Turns per coil	6
Coils per pole per phase	4
Rotor Outer diameter	131 mm
Rotor Inner diameter	45 mm
Air gap Length	1 mm
Magnet Thickness	2.6 mm
Magnet Width	21.33 mm

Table 2: Slot Data for Different Geometries

	Small	Original	Large	High
H _{slot} (%)	85	100	115	115
W _{slot} (%)	85	100	100	115
A _{slot} (mm ²)	62.5	86.5	99.48	114.4
A _{cu} (mm)	27.23	71.4	49.84	42.65

Table 3: Material of machine parts, and data reference

Part	Material	
Frame	Aluminum Alloy 195	[18]
Lamination	NO30, Tata Cogent	[18]
Winding	Copper	[18]
Winding Impregnation	Unsaturated Polyester	[18]
Magnets	N30UH	[18]

The maximum dc voltage is 400 V, and the maximum rms phase current is 251 A in all four situations to limit the influence on the inverter and battery throughout this experiment. The latter indicates that the maximum current density in the Small slot is the highest, while the maximum current density in the Large slot is the lowest.

Table 3 shows the materials that were chosen. Table 4 shows the mass of various motor parts with the Original slot machine. The Small slot machine is the one with the least copper and the most steel. Because copper is more costly per unit mass than laminations [19], the Small slot machine material should be the least expensive of the four.

Table 4: Mass (kg) of reference motor parts (original slot)

Motor Part	Weight (kg)
Stator Yoke	8.26
Stator Teeth	5.24
Active Winding	6.45
Magnets	1.965
Shaft	2.28
Bearings	0.4
Total	34.22

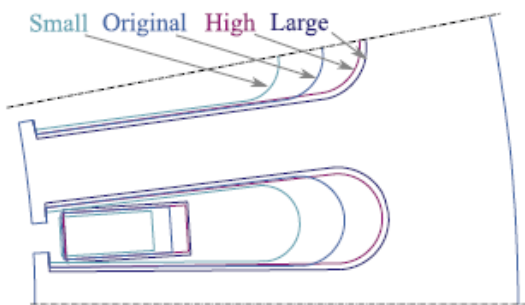


Fig. 2: different stator lamination geometries

III. FINITE ELEMENT ANALYSIS

In the electromagnetic finite element analysis (FEA) programmed Ansys Maxwell, machines with the four slot versions were simulated in 2D. Figure 1 depicts the simulated

machine shape and mesh density. In all electromagnetic models, the lamination stacking factor is omitted for simplicity.

Figure 3 depicts the FEA findings of the machine in question with its original slots (120° cut section).

As the slot area was increased, we saw that the no load input power and input active electrical power were gradually lowered, boosting the efficiency. With the rise in slot diameters, the loss of stator iron increased as well. Because of the increasing slot area, the effective core area is shrinking. The flux density is growing, which means more iron is being lost. Tables 5 and 6 summaries this information. For all of the slots investigated, Figure 4 depicts the change in stator tooth flux density.

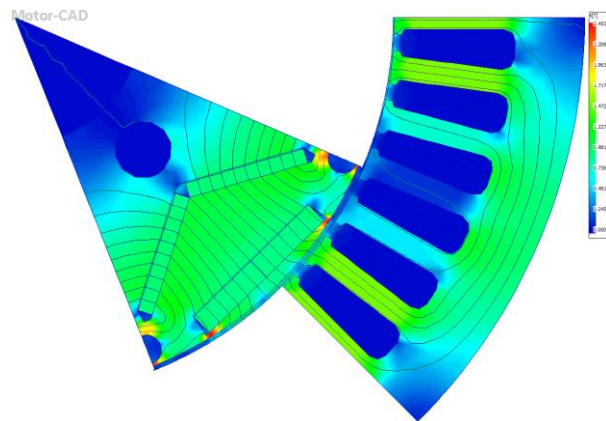


Fig. 3: Flux density in different parts of the original slot machine

Table 5: Input power, Output power and efficiency comparison

Parameters	Small	Original	Large	High
Shaft Torque (N-m)	110	114	105	112
Input Active Power (kW)	47.59	50.3	44.73	48.42
Output Mechanical Power (kW)	45.57	48.06	42.49	46.16
Efficiency	95.76	95.44	95.01	95.34

Table 6: Comparison of Stator and rotor losses

Parameters	Small	Original	Large	High
Stator Iron Loss (kW)	1.24	1.16	1.106	1.131
Stator Copper Loss (kW)	1.039	1.045	1.052	1.052
Rotor Iron Loss (kW)	0.08	0.06	0.05	0.05
Magnet Loss (kW)	0.004	0.004	0.003	0.002
Total Loss (kW)	2.277	2.296	2.227	2.254

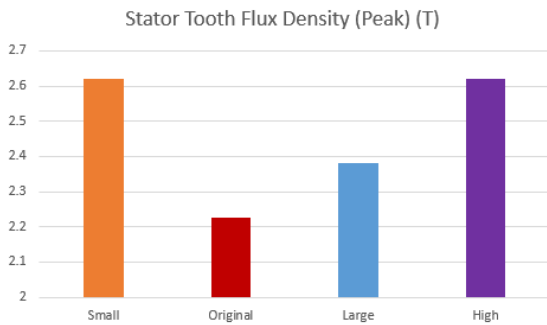


Fig. 4: Stator tooth flux density for different slot size

IV. THERMAL LUMPED PARAMETER NETWORK MODELLING

Internal heat generation is assumed to be equally distributed in each location, as in Refs. [27]. According to Ref. [27], axial heat transmission is considered in the copper windings and shaft, while only radial heat transfer is evaluated in the laminations and magnets. Furthermore, axial symmetry at the midway is expected, as well as geometric and thermal cylindrical symmetry. Radiative heat transmission is not taken into account.

Frame and Cooling:

For the current density employed, the machines are liquid cooled, as recommended in [30, p.90]. Because 50/50 Water Ethylene Glycol (WEG) is often used in BEVs [15], the coolant is a combination of 48 percent (by volume) water and 52 percent mono ethylene glycol [26].

$R_{th,Co Fr}$ is the sum of the resistances for the two primary heat transfer modes involved: convection between the coolant medium and the cooling duct walls, and conduction inside the frame. When compared to forced

convection, both natural convection to the ambient air and any sort of radiation are deemed insignificant [3].

$$R_{th,Fr} = \frac{\ln\left(\frac{r_{Fr,in} + l_{Fr,lower}}{r_{Fr,in}}\right)}{2\pi\lambda l}$$

$$R_{th,cool} = \frac{k_{conv,corr}}{h_{cool}A_{cool}}$$

$$R_{th,CO-Fr} = \frac{R_{th,cool} + R_{th,Fr}}{2}$$

Inside the aluminum frame, the cooling channel is created as a spiral of four laps, as shown in Fig. 5. The cooling ducts are rectangular in shape, with a width of 30 mm and a height of 5 mm, and are separated by 10 mm. On each side, the radial distances between the inner and outer frame limits $l_{Fr,lower}$ and the ducts are 3 mm.

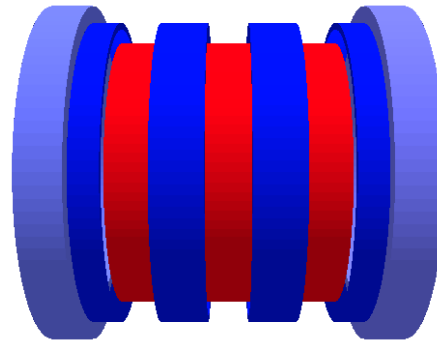


Fig. 5: Cooling channels with rectangular ducts

Stator Yoke:

The stator yoke thermal resistance $R_{th,StYo}$ is represented as a hollow cylinder made up of stacked laminated sheets of electrical steel with excellent insulation, as in [21, p.85], assuming a purely radial heat flow. Because of the stacking factor, the cylinder's length is less than the core's.

Stator Teeth:

In the stator teeth, only radial heat flow is considered, which is described as parallel thermal resistances. The total radial thermal resistance of the teeth $R_{th,Te}$ is calculated using the same approach as in [23, p.69e70] and [21, p.87e88]. The tooth width variation in the radial direction is then represented analytically.

Stator Winding:

The heat flow from the winding is substantial because copper losses are one of the primary loss components in motors. Not only the copper wires, but also the wire insulation, impregnation, air pockets, and the slot lining will be heated. A particular geometrical depiction is not

achievable since the scattered stranded winding is not geometrically well characterised.

Magnet and Rotor Yoke:

The very complicated magnet V-shape is substituted by an analogous geometry with arced magnets since only radial heat flow is addressed. A little air gap is also inserted beneath the magnet. The rotor's corresponding thermal resistance is then a combination of series and parallel connections.

$$R_{th,RoYo-Pm} = \frac{R_{th,magEq}}{2} + R_{th,magAG} + \frac{R_{th,Ros1}}{2}$$

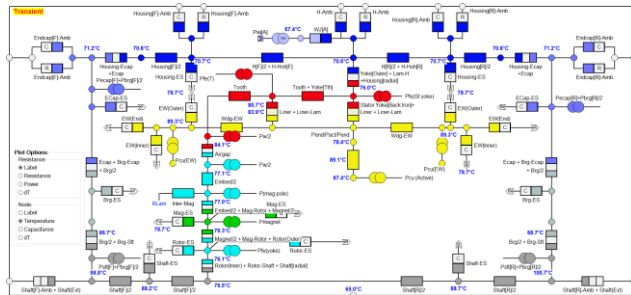


Fig. 6: Thermal LPN Model

V. STEADY STATE AND TRANSIENT PERFORMANCE

Figure 6 depicts the thermal network calculation technique, which has two types of inputs: first, a specified coolant temperature and flow rate, and second, motor torque and speed operating points. The electromagnetic losses in the six motor sections, as well as bearing losses, are then extracted for the precise operating locations.

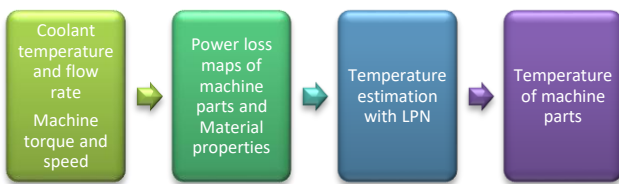


Fig. 7: Thermal performance evaluation process

When updating the motor losses for the current temperatures in the steady state solution for each operating point, an initial guess of the temperature in the winding network nodes is employed first, which is done by linear interpolation. The temperatures and losses are then updated with regard to each other in an iterative loop until the temperature difference between the last two iterations falls below a set threshold value.

Similarly to the steady state situation, an initial temperature assumption for the first value of the losses is

made in the transient solution. The temperature rise during a one-time step, on the other hand, is computed. The losses are temperature adjusted in the following time step by using the temperatures from the previous time step.

It is desirable to keep the maximum temperature in the windings of an electric machine to a minimum in order to extend the motor's lifetime. The critical temperature is determined by the winding insulation class as well as the design goal number of working hours [3].

The steady state research revealed that as the slot area was increased, the winding temperature and slot tooth temperature both decreased. Figure 8 illustrates this. The temperature of slot tooth and winding for small slot geometry is 1500C, whereas it is 1470C, 1460C, and 1450C for original, big, and high slot geometry, respectively.

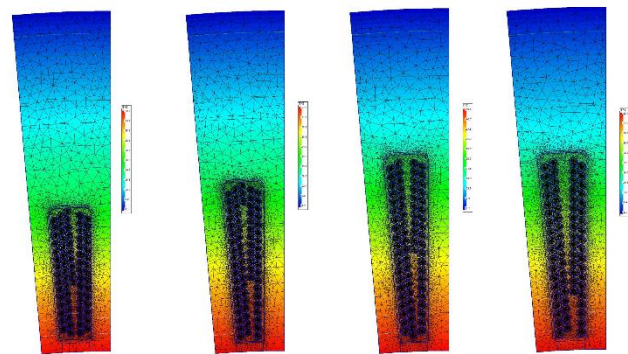


Fig. 8: Slot Tooth Temperature

Figure 9 shows the curve for when the winding achieves a temperature of 120°C to 170°C (insulation class H) for all four slot configurations. In comparison to the other slot geometries, the motor with the Small slot will attain the winding temperatures in a shorter amount of time. The Large slot shape allows for the longest running period at the stated temperatures. This is owing to the Substantial slot's reduced losses, particularly copper losses, in a large portion of the motor's operating area compared to the other geometries, and the Small slot's larger losses.

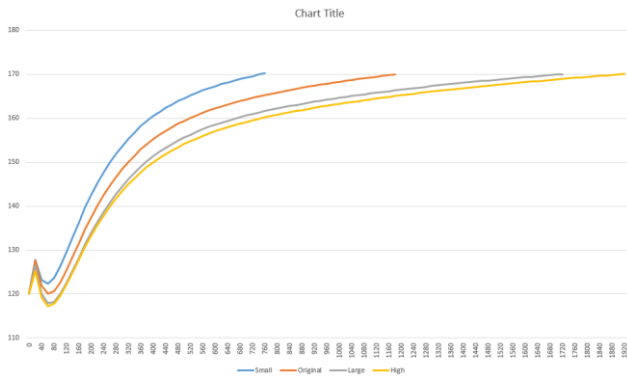


Fig. 9: Seconds spent in different operating points, before end winding reach 170 °C

The maximum time length in a given operating condition is computed for transient analysis. While the end winding has already reached 1200C in steady condition, the transient simulation is performed. As a starting point, the initial steady state temperatures of all motor components at this torque level are employed. The time it takes for the end winding to reach 170°C is then calculated using the transient thermal response, as shown in Fig. 9.

The Large slot geometry can be sustained for the greatest duration without overheating, as predicted by the steady state data. It takes 1920 seconds for the end winding to reach the critical temperature of 170°C in high slot geometry. It takes 1720 seconds for the Large slot to attain temperature, 1180 seconds for the Original, and 760 seconds for the Small slot.

VI. DRIVE CYCLE PERFORMANCE

On a flat road, the vehicle’s instantaneous longitudinal wheel force F_{wheel} is the sum of the aerodynamic force, the rolling resistance, and the acceleration force as in

$$F_{wheel} = \frac{1}{2} \rho C_d A v^2 + C_r \cdot m \cdot g + m \frac{dv}{dt}$$

where r is air density (1.2 kg/m³), v (m/s) is longitudinal vehicle speed, m (kg) is total rolling mass, g gravitational constant (9.81 m/s²). The used vehicle parameters are presented in Table 7.

Table 7: Vehicle Parameters

Part	Value	Unit
Weight	1521	kg
Front area	2.29	m ²
Wheel radius	0.3	M
Rolling resistance coefficient	0.007	-
Gear ratio	7.938	-

The wheel force relates to the electric machine torque T_{EM} and speed η_{EM} via the wheel radius r , the transmission gear ratio k_{gear} and its efficiency η_{gear} (97%), in motoring mode as

$$T_{EM} = \frac{r F_{wheel,PT}}{\eta_{gear} k_{gear}}$$

The temperature development of the motor during chosen driving cycles is evaluated and compared amongst the three stator designs using a coolant flow rate of 6 L/min at 65°C. Ref. [15] goes into much detail on the cycles. To obtain thermal stable state, the cycle is repeated numerous times. Figure 6 shows the motor component losses and temperature growth during US6 as an example. Copper losses are greater during the cycle's high-speed driving. During the breaking of the cycle, large power loss peaks occur, causing a temperature rise in the winding. Throughout the cycles, the shaft temperatures are the greatest.

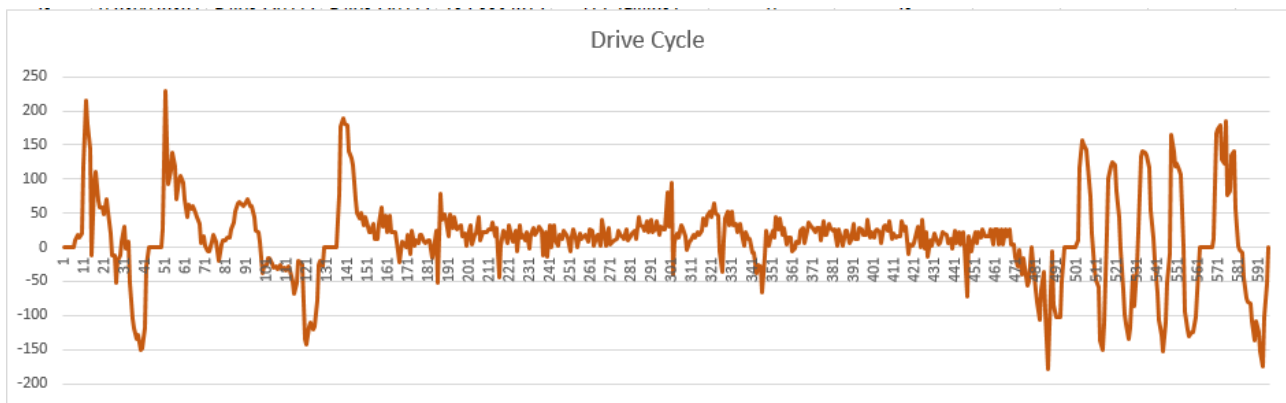


Fig. 10: Duty Cycle



Fig. 11: Losses occurred in the shaft

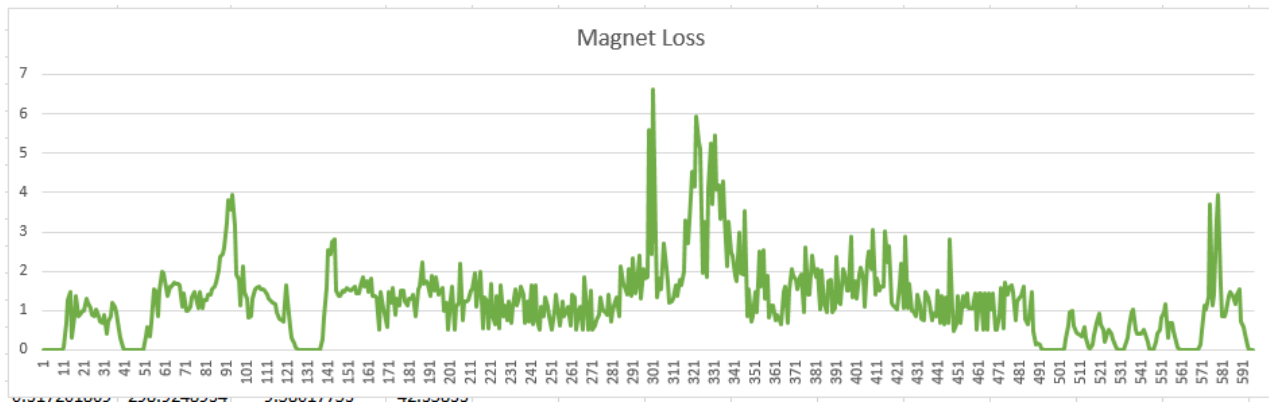


Fig. 12: Losses occurred in the Magnet

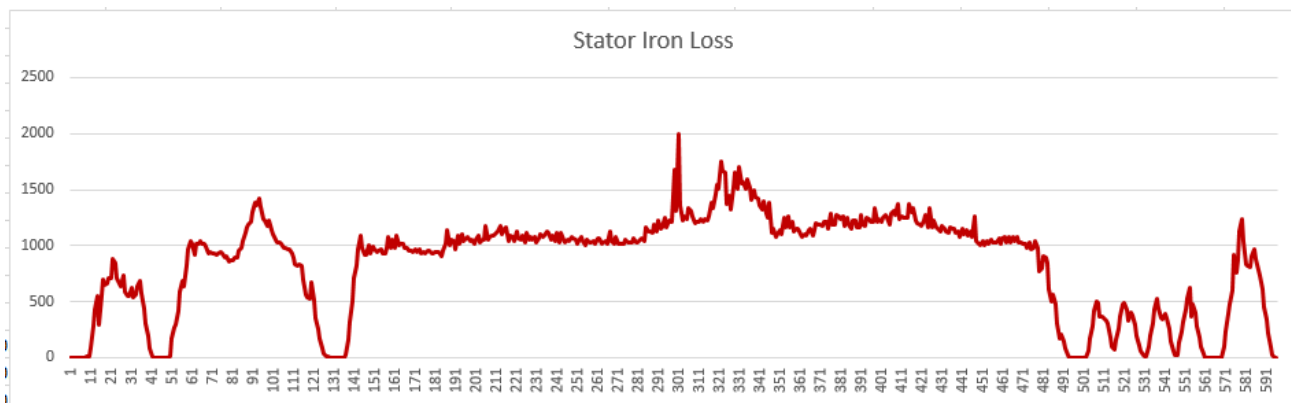


Fig. 13: Losses occurred in the Stator Iron

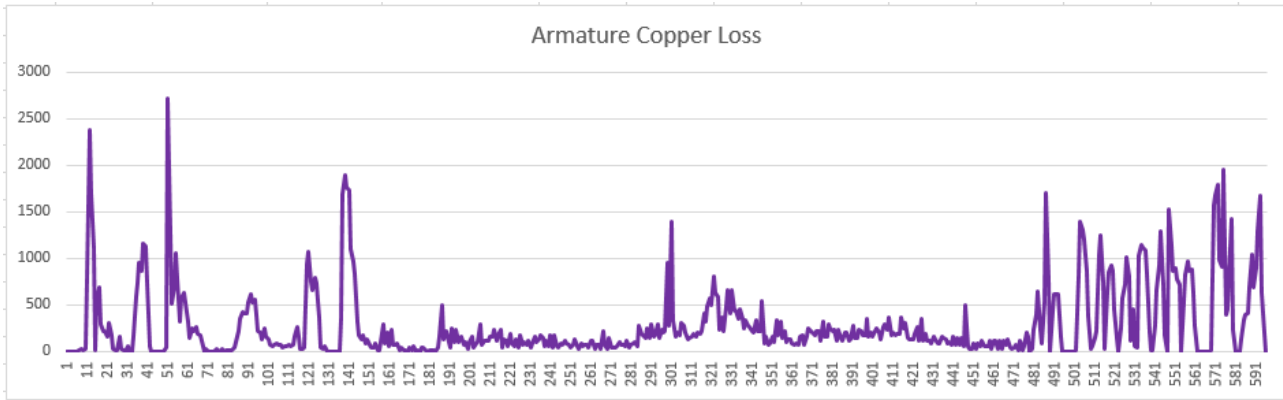


Fig. 14: Losses occurred in the Armature Copper

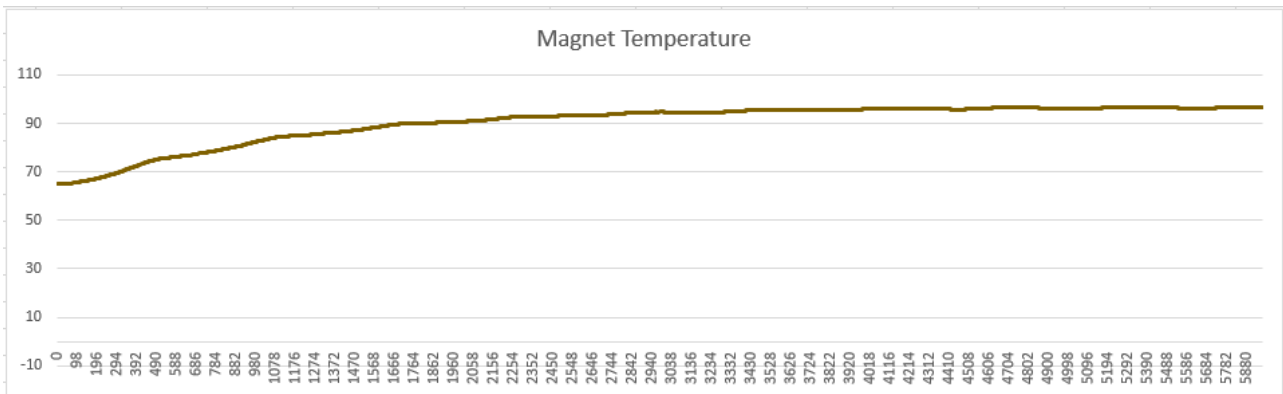


Fig. 15: Magnet temperature during 10 consecutive drive cycle

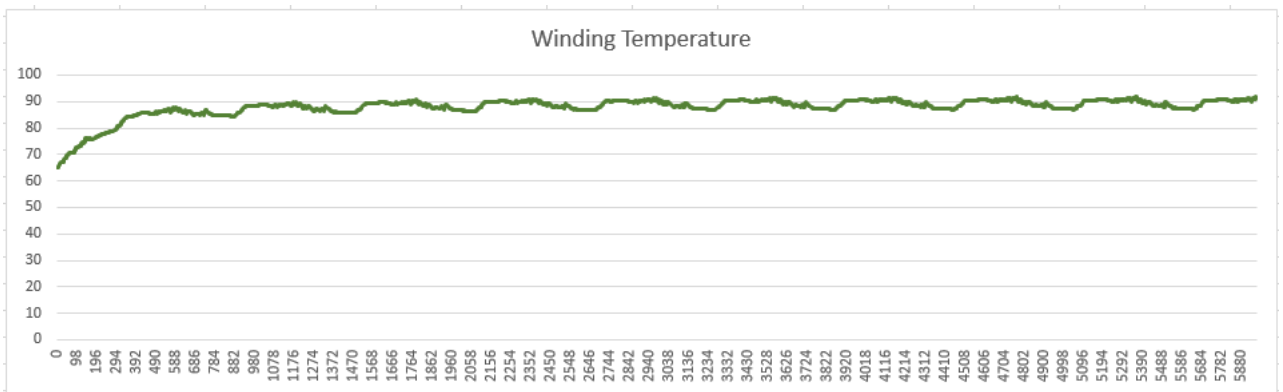


Fig. 15: Winding temperature during 10 consecutive drive cycle

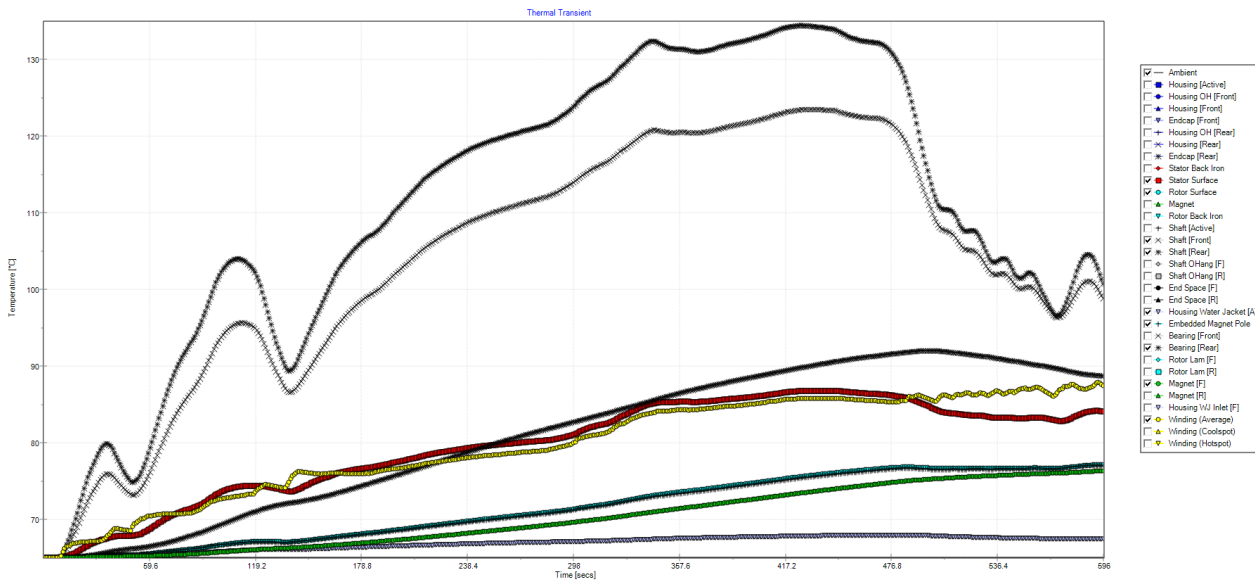


Fig. 15: Temperature rise of each part of the motor during drive cycle

VII. CONCLUSION

The goal of this research is to perform a focused electric machine design study that will be extremely useful in the creation of more purpose-built electric drive trains. The slot size (along with the copper area) for a PMSM reference motor is modified in this work while the gross fill factor, current and voltage ratings are maintained constant, resulting in a shift in the amount of losses between the winding and core. The electromagnetic and thermal performance of a machine with four different sized slot regions labelled Small, Original, High, and Large is assessed using FEA using a lumped parameter network model.

The paper's main contributions are to compare the part and total losses of the four machines in their torque-speed operating region, as well as their peak torque envelope at a certain magnet temperature. Second, a lumped parameter thermal network was used to estimate the continuous and transient overload torque capabilities of the four machines. Finally, during official drive cycles, to assess the machine's energy losses and attain peak winding and magnet temperatures.

A narrower slot, as predicted, increases copper losses and lowers iron losses (owing to a broader magnetic path), as well as increasing the peak torque generated for a given current rating. Because it contains the least copper, it would also result in a cheaper material cost. A bigger slot, on the other hand, has a greater thermally restricted continuous and transient overload torque capacity. The machine with the greatest slot area can maintain peak torque for 60 seconds, compared to 27 seconds, 38 seconds, and 13 seconds for the Original, High, and Small slot geometries, respectively.

Finally, despite the fact that this was a case study involving a specific machine, it is reasonable to assume that the trends in the data would hold true for similar machine types with similar dimensions. As a result, the choice of an appropriate electric machine design is inextricably linked to the individual application and its associated boundary conditions. As a result, the research described in this study is one viable way for quantifying similar features and evaluating optimization strategies.

VIII. REFERENCE

- [1] Khalifa, Fahim & Dessouky, Sobhy & Ismail, Mohamed & El Elnaghi, Basem. (2010). "Effect of Temperature Rise on the Performance of Induction Motors". Proceedings - The 2009 International Conference on Computer Engineering and Systems, ICCES'09. 549 - 552. 10.1109/ICCES.2009.5383074
- [2] Mellor P, Roberts D, Turner D. "Lumped parameter thermal model for electrical machines of tefc design", Electric Power Applications. IEE Proceedings B1991;138(5):205e18. <https://doi.org/10.1049/ip-b.1991.0025>.
- [3] Huang, Zhe & Marquez-Fernandez, Francisco & Loayza, Yury & Reinap, A. & Alakula, Mats. (2014). Dynamic thermal modeling and application of electrical machine in hybrid drives. Proceedings - 2014 International Conference on Electrical Machines, ICEM 2014. 2158-2164. 10.1109/ICELMACH.2014.6960483.
- [4] Boglietti, Aldo & Cavagnino, Andrea & Staton, D.. (2008). Determination of Critical Parameters in Electrical Machine Thermal Models. Industry Applications, IEEE

- Transactions on. 44. 1150 - 1159. 10.1109/TIA.2008.926233.
- [5] A. Fatemi, N. A. O. Demerdash, T. W. Nehl and D. M. Ionel, "Large-Scale Design Optimization of PM Machines Over a Target Operating Cycle," in *IEEE Transactions on Industry Applications*, vol. 52, no. 5, pp. 3772-3782, Sept.-Oct. 2016, doi: 10.1109/TIA.2016.2563383.
- [6] G. Y. Sizov, D. M. Ionel and N. A. O. Demerdash, "Multi-objective optimization of PM AC machines using computationally efficient - FEA and differential evolution," 2011 *IEEE International Electric Machines & Drives Conference (IEMDC)*, 2011, pp. 1528-1533, doi: 10.1109/IEMDC.2011.5994836.
- [7] Domingues-Olavarria, Gabriel & Marquez-Fernandez, Francisco & Fyhr, Pontus & Reinap, A. & Andersson, Mats & Alakula, Mats. (2018). Optimization of Electric Powertrains Based on Scalable Cost and Performance Models. *IEEE Transactions on Industry Applications*. PP. 1-1. 10.1109/TIA.2018.2864943.
- [8] Torres, C. & Garcia Espinosa, Antonio & Riba, Jordi-Roger & Romeral, Luis. (2017). Design and Optimization for Vehicle Driving Cycle of Rare-Earth-Free SynRM Based on Coupled Lumped
- [9] Thermal and Magnetic Networks. *IEEE Transactions on Vehicular Technology*. PP. 1-1. 10.1109/TVT.2017.2739020.
- [10] Martinovic, Marijan & Žarko, Damir & Stipetic, Stjepan & Jerčić, Tino & Kovačić, Marinko & Hanic, Zlatko & Staton, Dave. (2014). Influence of winding design on thermal dynamics of permanent magnet traction motor. 397-402. 10.1109/SPEEDAM.2014.6872026.
- [11] Huang, Yunkai & Zhu, Z.Q. & Guo, Baocheng & Lin, Heyun & Fang, Shuhua. (2016). Design and thermal analysis on high torque low speed fractional-slot concentrated windings in-wheel traction motor. 1487-1492. 10.1109/ICELMACH.2016.7732720.
- [12] Juergens, Jonathan & Brune, Andre & Ponick, Bernd. (2014). Electromagnetic design and analysis of a salient-pole synchronous machine with tooth-coil windings for use as a wheel hub motor in an electric vehicle. 744-750. 10.1109/ICELMACH.2014.6960264.
- [13] Redlich, Juergen & Juergens, Jonathan & Brune, Kai & Ponick, Bernd. (2017). Synchronous machines with very high torque density for automotive traction applications. 1-8. 10.1109/IEMDC.2017.8002283.
- [14] Wrobel, Rafal & Williamson, Sam & Simpson, Nick & Ayat, Sabrina & Yon, Jason & Mellor, P.H.. (2015). Impact of Slot Shape on Loss and Thermal Behaviour of Open-Slot Modular Stator Windings. 10.1109/ECCE.2015.7310286.
- [15] Emmrich, K. & Brune, Andre & Ponick, Bernd. (2014). Evaluation of an analytical, efficiency-optimized torque-speed characteristic of induction machines coupled with a thermal-electromagnetic energy consumption calculation. 762-767. 10.1109/ICELMACH.2014.6960267.
- [16] Goss, J. & Mellor, P.H. & Wrobel, Rafal & Staton, D.A. & Popescu, Mircea. (2012). The design of AC permanent magnet motors for electric vehicles: A computationally efficient model of the operational envelope. 2012. 1-6. 10.1049/cp.2012.0251.
- [17] Grunditz, Emma & Thiringer, T.. (2016). Performance Analysis of Current BEVs - Based on a Comprehensive Review of Specifications.